Hydrology and Earth System Sciences Discussions

Modelling catchment-scale shallow landslide occurrence by means of a subsurface flow path connectivity index

C. Lanni[1], M. Borga[2], R. Rigon[1], and P. Tarolli[2]

[1]Department of Civil and Environmental Engineering, University of Trento, Trento, Italy
[2]Department of Land and Agroforest Environments, University of Padua, Padua, Italy

Correspondence to: C. Lanni (cristiano.lanni@gmail.com)

Discussion Paper | Discussion Paper | Discussion Paper | Discussion Paper

HESSD

9, 4101–4134, 2012

Modelling catchment-scale shallow landslide occurrence

C. Lanni et al.

Title Page

Abstract	Introduction
Conclusions	References
Tables	Figures

◄ | ►

◄ | ►

Back | Close

Full Screen / Esc

Printer-friendly Version

Interactive Discussion

Abstract

Topographic index-based hydrological models have gained wide use to describe the hydrological control on the triggering of rainfall-induced shallow landslides at the catchment scale. A common assumption in these models is that a spatially continuous water table occurs simultaneously at any point across the catchment. However, during a rainfall event isolated patches of subsurface saturation form above an impeding layer and hydrological connectivity of these patches is a necessary condition for lateral flow initiation at a point on the hillslope.

Here, a new hydrological model is presented, which allows to account for the concept of hydrological connectivity while keeping the simplicity of the topographic index approach. A dynamic topographic index is used to describe the transient lateral flow that is established at a hillslope element when the rainfall amount exceeds a threshold value allowing for (a) development of a perched water table above an impeding layer, (b) hydrological connectivity between the hillslope element and its own upslope contributing area. A spatially variable soil depth is the main control of hydrological connectivity in the model. The hydrological model is coupled with the infinite slope stability model, and with a scaling model for the rainfall frequency-duration relationship to determine the return period of the critical rainfall needed to cause instability on three catchments located in the Italian Alps. The results show the good ability of our model in predicting observed shallow landslides. The model is finally used to determine local rainfall intensity-duration thresholds that may lead to shallow landslide initiation.

1 Introduction

Effective management of the hazard associated with shallow landsliding requires information on both the location of potentially unstable hillslopes and the conditions that cause slope instability. The need for spatial assessment of landslide hazard, along with the widespread use of Geographical Information Systems (GISs), has led to

Title Page

Abstract	Introduction
Conclusions	References
Tables	Figures

|◄ | ►|

◄ | ►

Back | Close

Full Screen / Esc

Printer-friendly Version

Interactive Discussion

the proliferation of mathematical, GIS-based, models (e.g., Montgomery and Dietrich, 1994; Pack et al., 1998; Borga et al., 2002; Baum et al., 2008) that can be applied over broad regions to assist forecasting, planning, and risk mitigation. Such models couple a hydrologic model, for the analysis of the pore-water pressure regime, with an infinite slope stability model for the computation of the Factor of Safety (i.e., the ratio of driving to resisting forces within the slope) at each point of a digitalized landscape.

In particular, with the increasing availability of digital elevation models (DEMs), the Topographic Wetness Index, TWI (Kirkby, 1975), computed from digital analysis as the ratio between specific upslope contributing area A/b (i.e., upslope contributing area, A, per unit contour length, b) and local slope angle $\tan\beta$ has been largely used as general indicator of the influence of topography on soil–water storage dynamics (e.g., Beven and Kirkby, 1979; Lanni et al., 2011) and shallow landslide triggering (e.g., Montgomery and Dietrich, 1994; Wu and Sidle, 1995; Casadei et al., 2003). SHALSTAB (Montgomery and Dietrich, 1994) and SINMAP (Pack et al., 1998) are among the most popular topography-based slope stability models, where the water table depth is computed based on a steady-state hydrologic balance, and it is expressed as a function of topographic wetness index. Borga et al. (2002) relaxed the hydrological steady-state assumption used in SHALSTAB by using a modified version of the quasi-dynamic wetness index developed by Barling et al. (1994). This allowed them to describe the transient nature of lateral subsurface flow under the assumption that a water table develops simultaneously at any point across the catchment (Grayson et al., 1997).

However, research in the last decade has shown that the establishment of hydrological connectivity (the condition by which disparate regions on the hillslope are linked via subsurface water flow, Stieglitz et al., 2003) is a necessary condition for lateral subsurface flow to occur at a point (e.g., Spence and Woo, 2003; Buttle et al., 2004; Graham et al., 2010; Spence, 2010). Lack of, or only intermittent, connectivity of subsurface flow systems invalidates the assumptions built into the TWI theory (i.e., the variable – and continuum – contributing area concept originally proposed by Hewlett and Hibbert, 1967). Field (e.g., Freer et al., 2002; Tromp van Meerveld and McDonnell, 2006) and

numerical (e.g., Hopp and McDonnell, 2009; Lanni et al., 2012) studies have shown that subsurface topography (and therefore soil-depth variability) has a strong impact in controlling the connectivity of saturated zones at the soil-bedrock interface, and in determining timing and position of shallow landslide initiation (Lanni et al., 2012). However, despite these evidences, most shallow landslide models fail to include a connectivity component for subsurface flow modelling.

Here, we propose a new topographic index-based shallow landslide model that includes the concept of hydrological connectivity in the description of the subsurface flow processes while keeping the simplicity of the topographic index approach needed to conduct large scale analysis. In our model, hydrological connectivity is preliminary related to the spatial variability of soil depth across the investigated catchments, and the initial soil moisture conditions. Vertical rain-water infiltration into unsaturated soil is simulated by using the concept of drainable porosity (i.e. the volume of stored soil-water removed/added per unit area per unit decline/growth of water table level – Hilberts et al., 2005). This allows simulating pore-water pressure dynamics under the assumption of quasi-steady state hydraulic equilibrium and to estimate the time for development of saturated conditions at the soil/bedrock interface. The model incorporates the computation of a characteristic time for describing the connection of these "patches" of saturation. Specifically, it is assumed that an element (x, y) in a hillslope connects (hydrologically) with its own upslope contributing area $A(x, y)$ when the water table forms a continuous surface throughout $A(x, y)$. Once hydrological connectivity is established, the dynamic topographic index developed by Lanni et al. (2011) is used to describe the transient subsurface flow converging in (x, y).

The hydrological model is then coupled with the infinite slope stability model to derive a shallow landslide model which is able to: (a) account for the (positive) effect of the unsaturated zone storage on slope stability, and (b) reproduce pre-storm unsaturated soil conditions. This implicitly helps reducing the fraction of catchment area categorized as unconditionally unstable, improving the confidence in model results (Keijsers et al., 2011).

Full Screen / Esc

Printer-friendly Version

Interactive Discussion

A critical rainfall intensity is computed by the model for a set of rainfall duration, which represents the hydrological conditions leading to hillslope instability. A scaling model for extreme rainfall is used to estimate the return period of the critical rainfall for shallow landsliding.

Model testing is carried out in three study sites located in the central Italian Alps. In this area, shallow landslides are generally triggered by local, convective storms during the summer and initial fall seasons. For these areas, accurate field surveys provide a description of hydraulic and geotechnical properties of soils and a detailed representation of soil depth variation as a function of local slope is reported. An inventory of shallow landslides is also available. Finally, the proposed shallow landslide model is used to derive local rainfall intensity-duration thresholds for the initiation of shallow landslides.

2 Materials and methods

2.1 The hydrological model

Figure 1 schematizes the hydrological model developed here. The model provides the pore pressure values at the soil-bedrock interface in each point of a hillslope.

In the model, during a rainfall event the formation of lateral flow is preceded by the development of positive pressure head (i.e. perched water table) at the soil-bedrock interface. Several researchers (McNamara et al., 2005; Rahardjo et al., 2005) have shown that infiltration through an unsaturated zone is vertical and (generally) causes no positive pore pressures. This vertical flow is reduced if the infiltration front meets a less permeable layer (for example, the bedrock layer) and the infiltration rate is larger than the permeability of this low-conductive layer. Under this condition, the infiltrating rainwater collects at the less permeable soil layer inducing rapid increases of pore-water pressure and unsaturated hydraulic conductivity (according to the relationship between matric suction head and unsaturated hydraulic conductivity). As a result, a perched

water table will form on the surface of the low-conductive layer, and a subsurface flow will move laterally along the upper surface of this layer (e.g., Weyman, 1973; Weiler et al., 2005). Moreover, in the model it is assumed that a generic hillslope element (x, y) receives flow from the related upslope catchment area $A(x, y)$ when isolated patches of transient saturation become connected with element (x, y) (Fig. 2).

According to field observations, unsaturated soil conditions through the whole soil-profile (i.e. positive suction head or negative pressure head) are used to initialize our model (step 1 in Fig. 1). For each hillslope element (x, y), the time $t_{wt}(x, y)$ needed to build up a perched zone of positive pore pressure at the soil-bedrock interface is computed by using the following expression (2 in Fig. 1):

$$t_{wt}(x, y) = \frac{V_{wt}(x, y) - V_0(x, y)}{I} \tag{1}$$

where V_0 [L] is the initial storage of soil moisture through the soil profile before of a rainfall event (Fig. 3); V_{wt} [L] is the storage of soil moisture needed to produce a perched water table (i.e., zero-pressure head) at the soil-bedrock interface (Fig. 3); and I [$L\,T^{-1}$] is the rainfall intensity. Computation of V_0 and V_{wt} require the use of a relationship between soil moisture content θ [–] and suction head ψ [L], and a relationship between ψ and the vertical coordinate (positive upward) z [L] (Fig. 3).

By using the assumption that the suction head profile $\psi(z)$ changes from one steady-state situation to another over the time, the relation between ψ [L] and z [L] is that of hydraulic equilibrium:

$$\psi = \psi(z = 0) + z = \psi_b + z \tag{2}$$

where $\psi_b = \psi(z = 0)$ is the suction head at the soil-bedrock interface. Bierkens (1998) argued that this assumption is valid for shallow system where redistribution of soil-water is rapid. Furthermore, comparisons with numerical models results described in Appendix A demonstrate that t_{wt} (the time needed to build up a perched zone of positive pore pressure at the soil-bedrock interface) computed by using our simplified approach

is similar to results from a one-dimensional Richards' equation solver (Fig. A1). The constitutive relationship between θ and ψ used in this study is the van Genuchten function (van Genuchten, 1980):

$$\theta(\psi) = \theta_r + (\theta_{sat} - \theta_r)\left[1 + (\alpha\psi)^n\right]^{-m} \tag{3}$$

with θ_{sat} [–] = saturated water content; θ_r [–] = residual water content; α [L^{-1}] = parameter that depends approximately on the air-entry (or air-occlusion) suction; n [–] and m [–] = van Genuchten parameters. Combining Eqs. (2) and (3) we obtain:

$$\theta(\psi) = \theta_r + (\theta_{sat} - \theta_r)\left[1 + (\alpha(\psi_b + z))^n\right]^{-m} \tag{4}$$

Troch et al. (1992) found that for the $\theta(\psi)$ relationship it is possible to assume the following relationship between m and n:

$$m = 1 + 1/n \tag{5}$$

instead of the common $m = 1 - 1/n$, without losing the ability to aptly fit the soil moisture retention data for a wide range of soil types. The storage of soil moisture through the soil profile V is obtained by integrating Eq. (4) from the bedrock to the ground surface:

$$V = \int_{z=0}^{z=L} \theta(z)\,dz = \theta_r \cdot L + (\theta_{sat} - \theta_r)\left[(L + \psi_b)\left(1 + (\alpha(L + \psi_b))^n\right)^{-\frac{1}{n}} - \psi_b\left(1 + (\alpha\psi_b)^n\right)^{-\frac{1}{n}}\right] \tag{6}$$

while V_{wt} can be obtained by setting zero-pressure head at the soil-bedrock interface ($\psi_b = 0$):

$$V_{wt} = \theta_r \cdot L + (\theta_{sat} - \theta_r) \cdot L \cdot \left(1 + (\alpha L)^n\right)^{-\frac{1}{n}} \tag{7}$$

Title Page

Abstract | Introduction

Conclusions | References

Tables | Figures

|◄ | ►|

◄ | ►

Back | Close

Full Screen / Esc

Printer-friendly Version

Interactive Discussion

The suction head value at the soil-bedrock interface at a generic time $t < t_{wt}(x,y)$ (i.e., before development of a perched water table), ψ_{b_t}, can be calculated by using the concept of drainable porosity f [–] proposed by Hilberts et al. (2005):

$$f = \frac{dV}{d\psi_b} = (\theta_{sat} - \theta_r) \cdot \left[\left(1 + (\alpha(L + \psi_b))^n \right)^{-1 - \frac{1}{n}} - \left(1 + (\alpha\psi_b)^n \right)^{-1 - \frac{1}{n}} \right] \tag{8}$$

By using Eq. (8), we can derive an expression for $d\psi_b/dt$, useful to estimate the suction head at the soil-bedrock interface at a generic time t, ψ_{b_t} (5a in Fig. 1):

$$\frac{d\psi_b}{dt} = \frac{I}{f} \overset{\text{implies}}{\Rightarrow} \psi_{b_t} = \psi_{b_{t-1}} + \frac{I}{(\theta_{sat} - \theta_r) \cdot \left[\left(1 + (\alpha(L + \psi_b))^n \right)^{-1 - \frac{1}{n}} - \left(1 + (\alpha\psi_b)^n \right)^{-1 - \frac{1}{n}} \right]} \tag{9}$$

For $t \geq t_{wt}(x,y)$, the generic hillslope element (x,y) exhibits a perched water table at the soil-bedrock interface.

However, this does not guarantee the hydrological connectivity between element (x,y) and its related upslope contributing area $A(x,y)$. In fact, due to the heterogeneity of initial soil-moisture and soil depth, isolated patches of saturation which do not necessarily connect with point (x,y) may have developed inside $A(x,y)$. We assume that lateral subsurface flow affects the local soil-water storage of point (x,y) when the water table time t_{wt} indicates continuous saturation through $A(x,y)$. Thus, each point (x,y) has two water table characteristic times: (1) t_{wt}, which indicates the local time for the development of a perched water table; and (2) a connectivity time t_{wt}^{up} – given by the maximum value of t_{wt} in $A(x,y)$ – which indicates the time required by element (x,y) to become hydrological connected with $A(x,y)$. Therefore, a generic hillslope element (x,y) receives flow from its own upslope contributing area starting from $t = t_{wt}^{up}(x,y)$) (3 and 4b in Fig. 1). Details on the formulation of the connectivity time t_{wt}^{up} are given in Appendix B.

The incoming lateral flow in element (x, y) is then calculated by using the upslope contributing area $A(x, y)$ as a surrogate for lateral flow. In particular, we use the method proposed by Lanni et al. (2011) to describe a variable upslope contributing area which changes linearly with time:

$$A_t(x, y) = \frac{t - t_{\text{wt}}^{\text{up}}(x, y)}{\tau_c(x, y)} A(x, y) \quad \text{for} \quad t_{\text{wt}}^{\text{up}}(x, y) < t \leq \tau_c(x, y) \tag{10a}$$

$$A_t(x, y) = A(x, y) \quad \text{for} \quad \tau_c(x, y) \leq t \leq d \tag{10b}$$

$$A_t(x, y) = \max\left[0, A(x, y) \left(1 + \frac{d - t}{\tau_c(x, y) - t_{\text{wt}}^{\text{up}}(x, y)} \right) \right]$$
$$\text{for} \quad t \geq d \quad \text{if} \quad \tau_c(x, y) \leq d \tag{10c}$$

$$A_t(x, y) = \max\left[0, A(x, y) \left(1 + \frac{2d - t_{\text{wt}}(x, y) - t}{\tau_c(x, y) - t_{\text{wt}}^{\text{up}}(x, y)} \right) \right]$$
$$\text{for} \quad t_{\text{wt}}^{\text{up}}(x, y) < t < d \quad \text{if} \quad \tau_c(x, y) \leq d \tag{10d}$$

where A_t and A are, respectively, the time-variable upslope contributing area and the (steady-state) upslope contributing area; t [T] = time; d [T] = rainfall duration; τ_c [T] = time of concentration (i.e., the time required for a drop of water to travel from the most hydrologically remote location in the subcatchment $A(x, y)$ to the (x, y) point under investigation). τ_c is defined as the maximum ratio between the flow-path length and the celerity of water given by Darcy's law added to the connectivity time for lateral

subsurface flow commencement $t_{\text{wt}}^{\text{up}}(x, y)$:

$$\tau_{\text{c}}(x, y) = \left\{ \frac{l_{H_j}(x, y)}{\cos\left(\beta_{l_{H_j}}(x, y)\right)} \frac{\Phi_{l_{H_j}}(x, y)}{K_{\text{sat}_{l_{H_j}}}(x, y) \cdot \sin\left(\beta_{l_{H_j}}(x, y)\right)} \right\} + t_{\text{wt}}^{\text{up}}(x, y) \qquad (11)$$

with $j = 1, \dots,$ number of flow paths converging in point (x, y)

where $\beta_{l_{H_j}}(x, y)$ [°] is the average inclination angle of the j-th flow path, of horizontal length l_{Hj} [L], which converges in the (x, y) catchment-point, while $\Phi_{l_{Hj}}(x, y)$ [–] and $K_{\text{sat}_{l_{Hj}}}(x, y)$ [LT^{-1}] are the average soil-porosity and saturated hydraulic conductivity along the j-th flow path, respectively.

Therefore, under the assumptions of constant rainfall intensity I in time and space, the positive pore pressure value at the soil-bedrock interface of point (x, y) for a generic time $t \geq t_{\text{wt}}^{\text{up}}(x, y)$, $h_{b_t}(x, y)$ is given by (6b2 in Fig. 1):

$$h_{b_t}(x, y) = -\psi_{b_t}(x, y) = \min\left[\frac{I}{K_{\text{sat}}(x, y)} \cdot \frac{A_t(x, y)}{b(x, y) \cdot \sin[\beta(x, y)]}, L(x, y)\right] \qquad (12)$$

where β [°] is the local slope angle, and A_t/b [L] is the time-variable contributing area per unit contour length.

2.2 The coupled hydrological-slope stability model

For hillslopes it is common to define the safety factor as the ratio between maximum retaining forces, F_{r}, and driving forces, F_{d} :

$$\text{FS} = \frac{F_{\text{d}}}{F_{\text{r}}} \qquad (13)$$

The slope is stable for FS > 1, while slope failure occurs when the critical state FS = 1 (such that $F_{\text{r}} = F_{\text{d}}$) is achieved. Lu and Likos (2006) derived a formulation to compute

Title Page

Abstract | Introduction

Conclusions | References

Tables | Figures

◄◄ | ►►

◄ | ►

Back | Close

Full Screen / Esc

Printer-friendly Version

Interactive Discussion

the factor of safety of an infinite slope model that accounts for saturated/unsaturated zones. If the failure surface is located at the soil-bedrock interface, then the Lu and Likos' factor of safety can be written as:

$$FS = \frac{2 \cdot c'}{\gamma \cdot L \cdot \sin[2\beta]} + \frac{\tan \phi'}{\tan \beta} + S_e(\psi_b) \frac{\gamma_w}{\gamma} \frac{\psi_b}{L} (\tan \beta + \cot \beta) \cdot \tan \phi'$$

$$\text{for} \quad \psi_b > 0 \quad (h_b < 0) \tag{14a}$$

$$FS = \frac{2 \cdot c'}{\gamma \cdot L \cdot \sin[2\beta]} + \frac{\tan \phi'}{\tan \beta} + \frac{\gamma_w}{\gamma} \frac{\psi_b}{L} (\tan \beta + \cot \beta) \cdot \tan \phi'$$

$$\text{for} \quad \psi_b \leq 0 \quad (h_b \geq 0) \tag{14b}$$

with c' [FL^{-2}] = effective soil cohesion; ϕ' [°] = effective soil frictional angle; γ_w and γ [FL^{-3}] = volumetric unit weight of water and soil, respectively; S_e [–] = relative saturation degree. Equation (15) allows taking into account for the (positive) role played by suction head on the hillslopes stability. In this work, locations that are neither unconditionally unstable (i.e., locations that are unstable under the minimum soil-moisture conditions) or unconditionally stable (i.e., locations that are stable when saturated) will be called conditionally unstable as proposed in the pioneer work of Montgomery and Dietrich (1994).

By coupling the hydrological model (Eqs. 9 and 12) with the slope stability model (Eq. 14) the factor of safety for conditionally unstable locations (x, y) at a generic time t

reads:

$$\mathrm{FS}_t(x,y) = \frac{2 \cdot c'(x,y)}{\gamma \cdot L \cdot \sin[2\beta(x,y)]} + \frac{\tan \phi'(x,y)}{\tan \beta(x,y)}$$
$$+ S_e\left(\psi_{b_t}(x,y)\right) \frac{\gamma_w(x,y)}{\gamma(x,y)} \frac{\psi_{b_t}(x,y)}{L(x,y)} (\tan \beta(x,y) + \cot \beta(x,y)) \cdot \tan \phi'(x,y)$$
$$\text{for} \quad \psi_{b_t}(x,y) > 0 \quad \left(h_{b_t}(x,y) < 0\right) \tag{15a}$$

$$\mathrm{FS}_t(x,y) = \frac{2 \cdot c'(x,y)}{\gamma \cdot L \cdot \sin[2\beta(x,y)]} + \frac{\tan \phi'(x,y)}{\tan \beta(x,y)}$$
$$+ \frac{\gamma_w(x,y)}{\gamma(x,y)} \frac{I}{K_{\mathrm{sat}}(x,y) \cdot L(x,y)} \frac{A_t(x,y)}{b(x,y) \cdot \sin \beta(x,y)} (\tan \beta(x,y) + \cot \beta(x,y)) \cdot \tan \phi'(x,y)$$
$$\text{for} \quad \psi_{b_t}(x,y) \leq 0 \quad \left(h_{b_t}(x,y) \geq 0\right) \tag{15b}$$

2.3 Intensity-Duration-Frequency relationship for extreme rainfall events

The variability of rainfall intensity with rainfall duration for a specified frequency level is often represented by the Intensity-Duration-Frequency (IDF) relationship proposed by Koutsoyiannis et al. (1998):

$$I_F(d) = \varsigma_F \cdot d^{m_F - 1} \tag{16}$$

with $I_F(d)$ = rainfall intensity that can be exceeded with a probability of $(1 - F)$. ς_F and m_F are parameters estimated by least squares regression of $I_F(d)$ against rainfall duration d. It has been shown (Burlando and Rosso, 1996) that a Gumbel simple scaling model describes well the distribution of annual maximum series of rainfall in the Central Italian Alps. Based on this model, the rainfall intensity $I_F(d)$ can be determined as:

$$I_F(d) = \varsigma_1 \left[1 - \frac{\mathrm{CV}\sqrt{6}}{\pi} \left(\varepsilon + y_{T_R} \right) \right] \cdot d^{m-1} \tag{17}$$

Modelling catchment-scale shallow landslide occurrence

C. Lanni et al.

with ε = Euler's constant (~ 0.5772). ς_1 and m can be estimated by linear regression of expectations of rainfall depth against duration, after log transformation, whereas the value of the coefficient of variation CV can be obtained as the average of coefficients of variation computed for the different durations, in the range of durations for which the scaling property holds. y_{T_R} is given by:

$$y_{T_R} = \ln\left(\ln\left(\frac{T_R}{T_R - 1}\right)\right) \tag{18}$$

where T_R [T] is the return period. By combining Eqs. (17) and (18), T_R can be written as a function of rainfall intensity and duration:

$$T_R = \frac{\exp\left[\exp\left[\frac{\pi}{CV\sqrt{6}}\left(1 - \varsigma_1 \frac{I_F(d)}{d^{m-1}}\right) - \varepsilon\right]\right]}{\exp\left[\exp\left[\frac{\pi}{CV\sqrt{6}}\left(1 - \varsigma_1 \frac{I_F(d)}{d^{m-1}}\right) - \varepsilon\right]\right] - 1} \tag{19}$$

2.4 Study sites and model application

The study area is represented by three small catchments located in the central Italian Alps: Cortina, Fraviano, and Pizzano catchments (Fig. 4). The overall surface of the three catchments is 7.5 km^2. Elevations (E) range from 1250 to 2830 m a.s.l., with an average value of 1999 m a.s.l. Average slope is 28°, almost identical between the three catchments. 10 m-resolution DEMs for the three catchments were derived from a 1:10,000 scale contour map. The shallow landslides analyzed in this work were mapped in the period between 2000 and 2003, and were triggered by several rainfall events, in particular by relatively short duration events occurred during the falls of 2000 and 2002. Vegetation covers 82.4 % of the Cortina catchment, consisting of forest stands (74.2 %) and grassland (8.2 %), while the remaining part is unvegetated soils. The Fraviano catchment presents a higher portion of grassland (24.3 %) than

the Cortina catchment. The forest stands cover 55.3 %, while remaining areas are un-vegetated soil. Land use of the Pizzano catchment is similar to that observed for the Fraviano catchment.

Soil depth, topographic curvature and local slope were surveyed at a total of 49 points within the three subwatersheds. Survey locations were chosen to represent the range of topographic variation in the areas of model application. At each location two or three soil depth replicates 2–3 m apart were collected by driving a 150 cm long 1.27 cm diameter sharpened copper coated steel rod graduated at 5 cm interval vertically into the ground using a fence post pounder until refusal. The advantage of the depth to refusal method is that it is a direct and simple measurement of soil depth. It is inexpensive, albeit laborious and time consuming and limited to depths to which a rod can be pounded. A disadvantage is that the measurement is biased to underestimating the actual depth to bedrock, since there is uncertainty as to what actually causes refusal. Rocks and gravel that occur as residual relicts from weathering or colluvium may limit the rod penetration resulting in underestimation of soil depth.

The field measurements allowed us to derive the following relationship between soil depth L and local slope angle $\tan\beta$:

$$L = 1.006 - 0.85 \cdot \tan\beta \quad \text{for} \quad 0° \leq \beta \leq 45° \tag{20a}$$

$$L = 0 \quad \text{for} \quad \beta \geq 45° \tag{20b}$$

for $E < 2000$ m a.s.l.

$$L = 1.006 - 0.85 \cdot \tan\beta \quad \text{for} \quad 0° \leq \beta \leq 40° \tag{20c}$$

$$L = 0 \quad \text{for} \quad \beta \geq 40° \tag{20d}$$

for $E \geq 2000$ m a.s.l.

In fact, locations with local slope angle larger than 45° (below 2000 m) and 40° (above 2000 m) are characterized by rocky outcrops or very shallow soil thickness. Other topographic variables, such as plan curvature and specific catchment area, and land cover attributes showed no statistically significant relationship with soil depth. The

relationship between soil depth and slope identified for the study watersheds are consistent with findings reported in the literature (Saulnier et al., 1997; Tesfa et al., 2009).

The landslide area amounts to 1.4 % of the total area for the Cortina and Fraviano catchments and to 1.2 % of the total area for the Pizzano catchment. An intensive field campaign was carried out in the area during the summer season 2003, leading to the estimation of the hydraulic and mechanical soil-parameters reported in Table 1. The soil properties are assumed to be the same for all the three catchments. Although the forest stands cover more than 50 % of the areas, the soils in the basins can be considered cohesionless or only slightly cohesive.

The soil-moisture initial conditions were assumed to represent average climatic conditions based on estimated evapotranspiration fluxes and interstorm duration statistics, which are typical of the seasons where shallow landslides were recorded (summer season and first half of the fall season). These unsaturated soil moisture conditions correspond to considerable cohesion which is due to capillarity, as conceptualized in the generalized principle of effective stress (Lu and Godt, 2008; Godt et al., 2009).

We used the procedure reported by Borga et al. (2005) to estimate the following scaling parameters of the IDF relationship (Eq. 18): CV = 0.42, m = 0.48, ς_1 = 13.7 mm h$^{1-0.48}$.

Two general procedures may be considered for model application: diagnostic and predictive (Rosso et al., 2006). With the first procedure, terrain stability is simulated for a given temporal pattern of rainfall intensity and for given initial soil moisture conditions. This allows exploration of the pattern of instability generated by specific storms and could be used to make real-time forecast of shallow landslides. The predictive procedure – able to provide a map of shallow landslide susceptibility – is adopted in this work. First, the critical duration d_c of rainfall which generates instability (i.e. FS = 1) is computed for a range of constant rainfall intensity I (5, 10, 15, 20, 25, 30, 35, 40, 45, 50, 55, 60 mm h^{-1}). Then, the return period T_r is computed for each (I, d_c) pair analyzed by using Eq. (20). Finally, the lowest return period for each conditionally stable

Modelling catchment-scale shallow landslide occurrence

C. Lanni et al.

Title Page

Abstract | Introduction

Conclusions | References

Tables | Figures

◄ | ►

◄ | ►

Back | Close

Full Screen / Esc

Printer-friendly Version

Interactive Discussion

location is selected. The map of the return period of the critical rainfall will provide a representation of the susceptibility to shallow landsliding across the landscape.

3 Results and discussion

By using the predictive procedure discussed in the previous paragraph, we derived the shallow landslide susceptibility map of Fig. 5. The criterion of shallow landslide susceptibility is based on the return period of the critical rainfall: higher return period values represent medium (T_r = 30–100 yr) and low (T_r > 100 yr) shallow landslide propensity, lower return period values represent high (T_r = 10–30 yr) and very high (T_r < 10 yr) shallow landslide propensity. A "very low" level of shallow landslide susceptibility is assigned to unconditionally stable points (i.e., locations that are stable when completely saturated, or characterized by bedrock outcrop). Examination of this map reveals that topographic elements in the steep areas close to the river are classified with a "very high" level of shallow landslide susceptibility (T_r < 10 yr). Conversely, higher values of critical return period T_r are found in gentle slope areas.

3.1 Assessment of shallow landslide susceptibility

Analysis of the results indicates the good ability of our model to assess the shallow landslide propensity at the three investigated sites.

The assessment of the predictive power of the model is carried out by mapping the observed landslides onto the map of return period of critical rainfall necessary for slope instability and by comparing the resulting patterns. Table 2 shows the proportion of catchment area placed in the intervals of critical return period and the corresponding fraction of the landslide area. Better model performances are reflected by a larger difference between fractions of catchment, and observed landslide areas corresponding to low values of return period. For example, for the Pizzano basin the percentage of catchment area with a frequency of critical rainfall in the range of 0–10 yr is equal to

Full Screen / Esc

Printer-friendly Version

Interactive Discussion

1.6 % (30.3 % in the range of 10–30 yr), while the corresponding fraction of observed landslide area is equal to 51.6 % (41.4 % in the range of 10–30 yr). On the other hand, the percentage of landslide area with a frequency of critical rainfall > 100 yr is only the 1.1 % versus the 49.3 % (including the locations classified as unconditionally stable) of the catchment area. Therefore, the model would be able to correctly classify with a high or very high level of shallow landslide susceptibility most of the observed landslide areas. This is confirmed by the results for the Cortina and the Fraviano catchments, with this last one showing the best model predictions (63.8 % of landslide area falling in the 2.5 % of catchment area with $T_r \leq 10$ yr).

Our model did not predict unconditionally unstable locations (i.e., predicted to be unstable without rainfall). The contribute of negative pressure head (in Eq. 15a) ensured the stability of steeper topographic elements (i.e., locations with $\tan \beta \geq \tan \phi'$ for cohesionless soils) that would be otherwise classified as unconditionally unstable from traditional landslide models (e.g., Montgomery and Dietrich, 1994; Wu and Sidle, 1995; Pack, 1995; Borga et al., 2002; Tarolli et al., 2011) that do not account for the role of negative pressure head on soil-shear strength.

This is an interesting aspect of our investigation, since it helps to overcome the limitations of previous studies carried out in similar catchments without accounting for the hydrological processes in the unsaturated region. These limitations led to an over-representation of areas potentially subject to shallow landsliding, with relatively large percentage of catchment area included in unconditionally unstable areas. For example, neglecting the contribute of unsaturated soil-shear strength in Eq. (15) leads to classify the 15 % (~ 1.13 km^2) of our catchments as unconditionally unstable, against the only 0.11 km^2 of inventoried landslide area. This overrepresentation is particularly pronounced in the upper hillslope zones where high local slope values are present but, on the other hand, low upslope contributing areas (low recharge), high local slope itself (high downslope drainage), and the till soil layer (high evapo-transpiration rates) tend to maintain relatively dry (i.e., unsaturated) condition even during the year.

Modelling catchment-scale shallow landslide occurrence

C. Lanni et al.

Title Page

Abstract	Introduction
Conclusions	References
Tables	Figures

◀ ▶

Back | Close

Full Screen / Esc

Printer-friendly Version

Interactive Discussion

Our results suggest that model predictions capture a high percentage of observed landslides, at the expenses of some overprediction of slope instability. However, over-prediction of slope instability has been observed in other applications of topographic index-based shallow landsliding models (e.g., Dietrich et al., 2001). As explained in Tarolli et al., 2011, overprediction may be due to the following causes: (i) inaccurate soil property data, (ii) legacy effects of previous landslides, (iii) limitation of the land-slide surveys. Moreover, in steep terrain, a 10 m DEM-grid size such as that used here may lead to underestimation of the local slope steepness controlling shallow landslid-ing. It is also likely that the representation of the soil as cohesionless everywhere in this landscape may be responsible for overprediction of areas characterized by low return period.

3.2 Derivation of local rainfall thresholds for shallow landslide initiation

Once we verified the capability of our topographic index-based shallow landslide model to assess the shallow landslide propensity at the investigated sites, we used our model to derive local rainfall intensity-duration thresholds for shallow landslide initiation (Frat-tini et al., 2009). Because of the reduced computational cost, our model allowed us to perform a large number of numerical simulations in a very short time. We investigated 12 different constant value of rainfall intensity (I = 5, 10, 15, 20, 25, 30, 35, 40, 45, 50, 55, 60 mm h^{-1}). For each of these investigated cases, the coupled hydrological-slope stability model of Eq. (18) allowed us to determine the critical rainfall duration d_c needed to cause slope instability (i.e., FS=1). Figure 6 shows the results obtained by plotting the rainfall intensity (ordinate axis) against the critical rainfall duration (ab-scissa axis) in a log-log graph (gray points). The lower envelope curve $I = 14.58 \cdot d_c^{-0.80}$ has been chosen as a $I - d_c$ cautious threshold and may be used to forecast the oc-currence of shallow landslides at the investigated sites based on continuous rainfall measurements.

In Fig. 6, we also compare our $I - d_c$ lower envelope with rainfall features that trig-gered debris flow (filled circles in black) in some alpine catchments of the Dolomities.

These catchments are geologically similar to our study area, and we refer the reader to Gregoretti and Dalla Fontana (2008) for further details on the empirical rainfall intensity–duration threshold. Modeled threshold is in good agreement with experimental threshold, proving that our $I - d_c$ cautious threshold may be used to forecast the occurrence of shallow landslides for the area of application.

4   Summary and conclusions

The shallow landslide model developed here is appealing for investigating the relation between the spatial occurrence of shallow landslides and characteristics of the triggering rainfall events, as it estimates the local pore pressure values by accounting for both vertical infiltration in unsaturated soil and lateral flow in the saturated zone.

A procedure to assess shallow landslide susceptibility was presented by coupling the proposed shallow landslide model with Intensity-Duration-Frequency (IDF) relationships of extreme rainfall events. This procedure is based on the idea that lateral flow occurs when a connectivity time for lateral subsurface flow initiation is achieved. This connectivity time represents the time-lag (from the onset of rainfall) required for a point in the basin to become hydrologically connected with its own upslope contributing area. For time less than the connectivity time, vertical infiltration is simulated by using the concept of drainable porosity under the assumption of quasi-steady state hydraulic equilibrium. For time greater than the connectivity time, a dynamic topographic index allows to describe the transient lateral flow dynamics. Therefore, unlike the traditional, lateral flow-dominated, topographic index-based models, our model is able to account for the effects of partially saturated soil suction stress on slope stability.

Model performance was evaluated over three catchments located in the central Italian Alps, where detailed inventories of shallow landslides are available. We found that in all case studies model provides a reasonably correct surrogate for failure initiation probability. Once we verified the capability of the model to assess shallow landslide propensity, we used our model to define a local relationship on rainfall intensity-duration

Modelling catchment-scale shallow landslide occurrence

C. Lanni et al.

thresholds for shallow landslide initiation. These thresholds may be useful for forecasting landslide occurrence in the study sites. The proposed methodology may be adopted in the other catchments of the region affected by shallow landsliding phenomena to produce ad-hoc intensity-duration thresholds. This will help decision makers to efficiently allocate resources and personnel in emergency-response situations, and will allow (a) alerting the general public to the potential landslide activity, (b) limiting the alert signal to specific areas.

Appendix A

Comparison of results of our simplified unsaturated vertical infiltration model with results of a one-dimensional Richards equation solver

To assess the error associated with the use of our simplified method to estimate the time t_{wt} (needed to build up a perched zone of positive pore pressure at the soil-bedrock interface), we compare results from our unsaturated infiltration model, with those from a one-dimensional Richards equation solver (HYDRUS-1D, Simunek et al., 2008).

50 numerical simulations were performed on a colluvial soil layer overlying impermeable bedrock. We explored the interplay between three factors: soil depth (four values: 0.25 m, 0.5 m, 0.75 m, and 1.0 m), rainfall intensity (three values: 10 mm h^{-1}, 20 mm h^{-1}, and 30 mm h^{-1}), and initial condition (hydrostatic pore pressure profile with seven values of suction head at the soil-bedrock interface ψ_b: 0.05 m, 0.15 m, 0.25 m, 0.40 m, and 0.50 m). The systematic parameter exploration is useful in illustrating differences in t_{wt} estimation across the reasonable range of soil depth, initial condition and rainfall intensity values.

We assumed the same material properties of the soil reported in Table 1. Relations between pressure head and hydraulic conductivity and soil-water content were described using the Mualem model (Mualem, 1976) and Eq. (3). The domain was discretized using a uniform node spacing of 0.02 m in the vertical direction.

Differences between t_{wt} computed with HYDRUS-1D and t_{wt} computed with our simplified infiltration model for the 50 investigated scenarios are shown in the three dimensional plot of Fig. A1. In general, differences are small and the highest differences are associated with high soil depth and initial suction head at the soil/bedrock interface, and low rainfall intensity.

Appendix B

Computation of the connectivity time t_{wt}^{up} as a time of subsurface hydrological connectivity

The connectivity time t_{wt}^{up} for each point(x, y) in the basin is calculated as follows: starting at each point in the basin, each flow path is traced downslope, recording the highest value of the water table time t_{wt} encountered along this flow path. This highest value is assigned to each new cell encountered downslope until a higher value is encountered. This can be done because of the use of the D8 flow algorithm which assumes that each cell has a unique downslope flow direction. Therefore, when a flow path $P2$ converges in a pre-processed path $P1$, $P2$ is terminated if it contains a water table time lower than the encountered water table time in $P1$. On the other hand, $P2$ continues downslope to modify $P1$ with the highest upslope water table time.

Thus each grid cell in the basin has both a t_{wt} value, which indicates the local time for the development of a perched water table, and a connectivity time t_{wt}^{up}, which defines when a cell is hydrologically connected with its own upslope contributing area.

References

Barling, R. D., Moore, I. D., and Grayson, R. B.: A quasi-dynamic wetness index for characterizing the spatial distribution of zones of surface saturation and soil water content, Water Resour. Res., 30, 1029–1044, 1994.

Baum, R. L., Savage, W. Z., and Godt, J. W.: TRIGRS– A FORTRAN program for transient rainfall infiltration and grid based regional slope stability analysis, version 2.0, US Geol. Surv. Open File Rep. 2008, 1159, 74 pp. 2008.

Beven, K. J. and Kirkby, M. J.: A physically based variable contributing area model of basin hydrology, Hydrology Science Bulletin, 24, 43–69, 1979.

Bierkens, M.: Modeling water table fluctuations by means of a stochastic differential equation, Water Resour. Res., 34, 2485–2499, 1998.

Borga, M., Dalla Fontana, G., and Cazorzi, F.: Analysis of topographic and climatologic control on rainfall-triggered shallow landsliding using a quasi-dynamic wetness index, J. Hydrol., 268, 56–71, 2002.

Borga, M., Dalla Fontana, G., and Vezzani, C.: Regional rainfall depth-duration-frequency equations for an alpine region, Nat. Hazards, 36, 221–235, 2005.

Burlando, P. and Rosso, R.: Scaling and multiscaling models of depth–duration–frequency curves from storm precipitation, J. Hydrol., 187, 45–64, 1996.

Buttle, J. M., Dillon, P. J., and Eerkes, G. R.: Hydrologic coupling of slopes, riparian zones and streams: an example from the Canadian Shield, J. Hydrol., 287, 161–177, 2004.

Casadei, M., Dietrich, W. E., and Miller, N. L.: Testing a model for predicting the timing and location of shallow landslide initiation in soil-mantled landscapes, Earth Surf. Proc. Land., 28, 925–950, 2003.

Dietrich, W. E., Bellugi, D., and Real de Asua R.: Validation of the shallow landslide model SHALSTAB for forest management, in: Land Use and Watersheds: Human Influence on Hydrology and Geomorphology in Urban and Forest Areas, edited by: Wigmosta, M. S. and Burges, S. J., American Geophysical Union Water Science and Application, 2, 195–227, 2001.

Frattini, P., Crosta, G., and Sosio, R.: Approaches for defining thresholds and return periods for rainfall-triggered shallow landslides, Hydrol. Process., 23, 1444–1460, 2009.

Title Page

Abstract | Introduction

Conclusions | References

Tables | Figures

◀◀ | ▶▶

◀ | ▶

Back | Close

Full Screen / Esc

Printer-friendly Version

Interactive Discussion

Freer, J., McDonnell, J. J., Beven, K. J., Peters, N. E., Burns, D. A., Hooper, R. P., Aulenbach, B., and Kendall, C.: The role of bedrock topography on subsurface storm flow, Water Resour. Res., 38, 1269, doi:10.1029/2001WR000872, 2002.

van Genuchten, M. T.: A closed-form equation for predicting the hydraulic conductivity of unsaturated soils, Soil Sci. Soc. Am. J., 44, 892–898, 1980.

Godt, J. W., Baum, R. L., and Lu, N.: Landsliding in partially saturated materials, Geophys. Res. Lett., 36, L02403, doi:10.1029/2008GL035996, 2009.

Graham, C. B., Woods, R. A., and McDonnell, J. J.: Hillslope threshold response to rainfall: (1) A field based forensic approach, J. Hydrol., 393, 65–76, 2010.

Grayson, R. B., Western, A. W., Chiew, F. H. S., and Blöschl, G.: Preferred states in spatial soil moisture patterns: local and nonlocal controls, Water Resour. Res., 33, 2897–2908, 1997.

Gregoretti, C. and dalla Fontana, G. D.: The triggering of debris flow due to channel-bed failure in some alpine headwater basins of the Dolomites: analyses of critical runoff, Hydrol. Process., 22, 2248–2263, doi:10.1002/hyp.6821, 2008.

Hewlett, J. D. and Hibbert, A. R.: Moisture and energy conditions within a sloping soil mass during drainage, J. Geophys. Res., 68, 1081–1087, 1963.

Hilberts, A., Troch, P., and Paniconi, C.: Storage-dependent drainable porosity for complex hillslopes, Water Resour. Res., 41, W06001, doi:10.1029/2004WR003725, 2005.

Hopp, L. and McDonnell, J. J.: Connectivity at the hillslope scale: identifying interactions between storm size, bedrock permeability, slope angle and soil depth, J. Hydrol., 376, 378–391, 2009.

Keijsers, J. G. S., Schoorl, J. M., Chang, K.-T., Chiang, S.-H., Claessens, L., and Veldkamp, A.: Calibration and resolution effects on model performance for predicting shallow landslide locations in Taiwan, Geomorphology, 133, 168–177, 2011.

Kirkby, M.: Hydrograph modelling strategies, in: Processes in Physical and Human Geography, edited by: Peel, R. F., Chisholm, M. D., and Haggett, P., Heinemann, London, 69–90, 1975.

Koutsoyiannis, D., Kozonis, D., and Manetas, A.: A mathematical framework for studying rainfall intensity–duration–frequency relationships, J. Hydrol., 206, 118–135, 1998.

Lanni, C., McDonnell, J. J., and Rigon, R.: On the relative role of upslope and downslope topography for describing water flowpath and storage dynamics: a theoretical analysis, Hydrol. Process., 25, 3909–3923, 2011.

Title Page

Abstract | Introduction

Conclusions | References

Tables | Figures

◀ | ▶

◀ | ▶

Back | Close

Full Screen / Esc

Printer-friendly Version

Interactive Discussion

Lanni, C., McDonnell, J. J., Hopp, L., and Rigon, R.: Hydrological controls on shallow landslide triggering: the role of soil depth and bedrock topography, provisionally accepted for publication in, Earth Surface Processes and Landforms, accepted, 2012.

Lu, N. and Godt J. W.: Infinite-slope stability under steady unsaturated seepage conditions, Water Resour. Res., 44, W11404, doi:10.1029/2008WR006976, 2008.

Lu, N. and Likos, W. J.: Suction stress characteristic curve for unsaturated soil, J. Geotech. Geoenviron. Eng., 123, 131–142, 2006.

McGuire, K. J. and McDonnell, J. J.: Hydrological connectivity of hillslopes and streams: Characteristic time scales and nonlinearities, Water Resour. Res., 46, W10543, doi:10.1029/2010WR009341, 2010.

McNamara, J. P., Chandler, D., Seyfried, M., and Achet, S.: Soil moisture states, lateral flow, and streamflow generation in a semi-arid, snowmelt-driven catchment, Hydrol. Process., 19, 4023–4038, 2005.

Montgomery, D. R. and Dietrich, W. E.: A physically based model for the topographic control on shallow landsliding, Water Resour. Res., 30, 1153–1171, 2010.

Mualem, Y.: A new model for predicting the hydraulic conductivity of unsaturated porous media, Water Resour. Res., 12, 513–522, 1976.

Pack, R. T., Tarboton, D. G., and Goodwin, C. N.: The SINMAP approach to terrain stability mapping, in: Proceedings – International Congress of the International Association for Engineering Geology and the Environment 8, v. 2, edited by: Moore, D. P. and Hungr, O., A. A. Balkema, Rotterdam, Netherlands, 1157–1165, 1998.

Rahardjo, H., Lee, T. T., Leong, E. C., and Rezaur, R. B.: Response of a residual soil slope to rainfall, Can. Geotech. J., 42, 340–351, doi:10.1139/t04-101, 2005.

Rosso, R., Rulli, M. C., and Vannucchi, G.: A physically based model for the hydrologic control on shallow landsliding, Water Resour. Res., 42, W06410, doi:10.1029/2005WR004369, 2006.

Saulnier, G. M., Beven, K., and Obled, C.: Including spatially variable effective soil depths in TOPMODEL, J. Hydrol., 202, 158–172, doi:10.1016/S0022-1694(97)00059-0, 1997.

Šimůnek, J., van Genuchten, M. T., and Šejna, M: The HYDRUS-1D software package for simulating the one-dimensional movement of water, heat, and multiple solutes in variably-saturated media, Version 4.0. HYDRUS Software Ser. 3. Dep. of Environmental Sciences, Univ. of California, Riverside, 2008.

Title Page

Abstract | Introduction

Conclusions | References

Tables | Figures

◀◀ | ▶▶

◀ | ▶

Back | Close

Full Screen / Esc

Printer-friendly Version

Interactive Discussion

Spence, C.: A paradigm shift in hydrology: storage thresholds across scales influence catchment runoff generation, Geography Compass, 4, 819–833, doi:10.1111/j.1749-8198.2010.00341.x, 2010.

Spence, C. and Woo, M. K.: Hydrology of subarctic Canadian shield: soil-filled valleys, J. Hydrol., 279, 151–166, doi:10.1016/S0022-1694(03)00175-6, 2003.

Stieglitz, M., Shaman, J., McNamara, J., Engel, V., Shanley, J., and Kling, G. W.: An approach to understanding hydrologic connectivity on the hillslope and the implications for nutrient transport, Global Biogeochem. Cy., 17, 1105, doi:10.1029/2003GB002041, 2003.

Tarolli, P., Borga, M., Chang, K.-T., and Chiang, S. H.: Modeling shallow landsliding susceptibility by incorporating heavy rainfall statistical properties, Geomorphology, 133, 199–211, 2011.

Tesfa, T. K., Tarboton, D. G., Chandler. D. G., and McNamara, J. P.: Modeling soil depth from topographic and land cover attributes, Water Resour. Res., 45, W10438, doi:10.1029/2008WR007474, 2009.

Troch, P., van Loon, E., and Hilberts, A.: Analytical solutions to a hillslope-storage kinematic wave equation for subsurface flow, Adv. Water Resour., 25, 637–649, 2002.

Tromp-van Meerveld, H. J. and McDonnell, J. J.: Threshold relations in subsurface stormflow: 2. The fill and spill hypothesis, Water Resour. Res., 42, W02411, doi:10.1029/2004WR003800, 2006.

Weiler, M., McDonnell, J. J., Tromp-van Meerveld, H. J., and Uchida, T.: Subsurface Stormflow, Encyclopedia of Hydrological Sciences, Wiley and Sons, 2005.

Weyman, D. R.: Measurements of the downslope flow of water in a soil, J. Hydrol., 20, 267–288, 1973.

Wu, W. and Sidle, R.: A distributed slope stability model for steep forested basins, Water Resour. Res., 31, 2097–2110, 1995.

Modelling catchment-scale shallow landslide occurrence

C. Lanni et al.

Title Page

Abstract	Introduction
Conclusions	References
Tables	Figures

|◄ | ►|

◄ | ►

Back | Close

Full Screen / Esc

Printer-friendly Version

Interactive Discussion

Table 1. Hydraulic and mechanical soil-parameters relative to the three investigated catchments.

Soil-parameter	Unit	Value
Density ratio (γ_s/γ_w)	[–]	1.8
Saturated water content θ_{sat}	[–]	0.3
Residual water content θ_r	[–]	0.05
α – van Genuchten	m^{-1}	3.44
n – van Genuchten	[–]	4.42
Saturated hydraulic conductivity K_{sat}	ms^{-1}	10^{-3}
Effective frictional angle ϕ	°	38
Effective cohesion c'	kPa	0

Title Page

Abstract | Introduction

Conclusions | References

Tables | Figures

|◀ | ▶|

◀ | ▶

Back | Close

Full Screen / Esc

Table 2. Percentages of slope-stability categories in terms of catchment area and observed landslide area in each range of critical rainfall frequency (i.e., return period T_R) or level of shallow landslide susceptibility.

T_R	Susceptibility Level	Pizzano		Fraviano		Cortina	
		C*	L**	C*	L**	C*	L**
Years	Category	%	%	%	%	%	%
0–10	Very High	1.6	51.6	2.5	63.8	3.8	24.3
10–30	High	30.3	41.4	26.9	36.2	24.2	75.7
30–100	Medium	18.0	5.9	22.1	0.0	26.3	0.0
> 100	Low	18.0	1.1	24.3	0.0	21.9	0.0
Uncond. stable	Very Low	32.1	0.0	24.2	0.0	23.8	0.0

* C = catchment area;
** L = landslide area

Title Page

Abstract | Introduction

Conclusions | References

Tables | Figures

|◄ | ►|

◄ | ►

Back | Close

Full Screen / Esc

Printer-friendly Version

Interactive Discussion
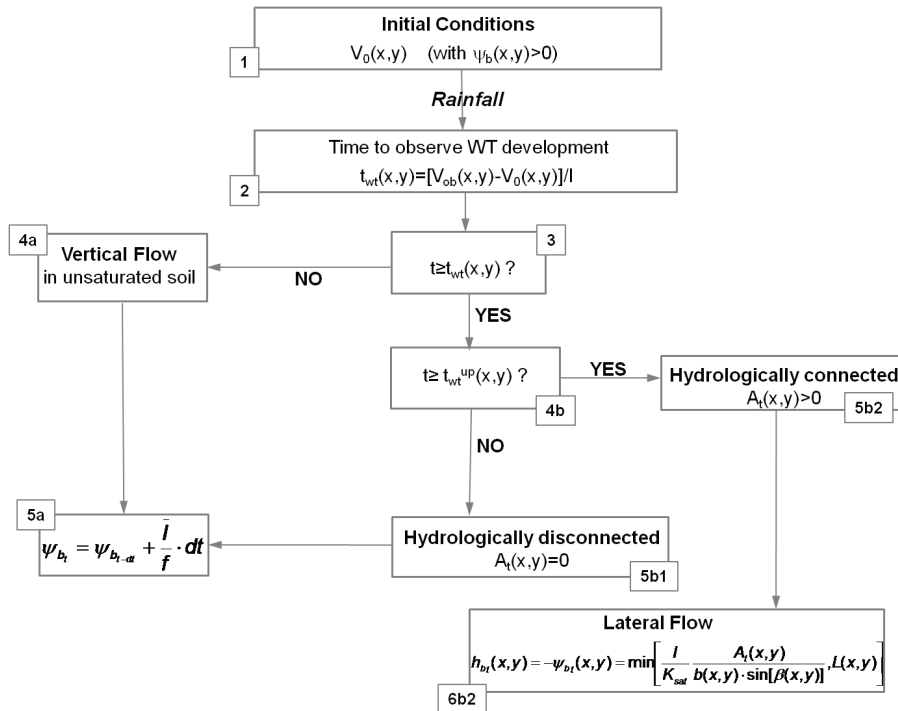
Fig. 1. A flow chart depicting the coupled saturated/unsaturated hydrological model developed in this study.

Title Page

Abstract | Introduction

Conclusions | References

Tables | Figures

|◄ | ►|

◄ | ►

Back | Close

Full Screen / Esc

Printer-friendly Version

Interactive Discussion
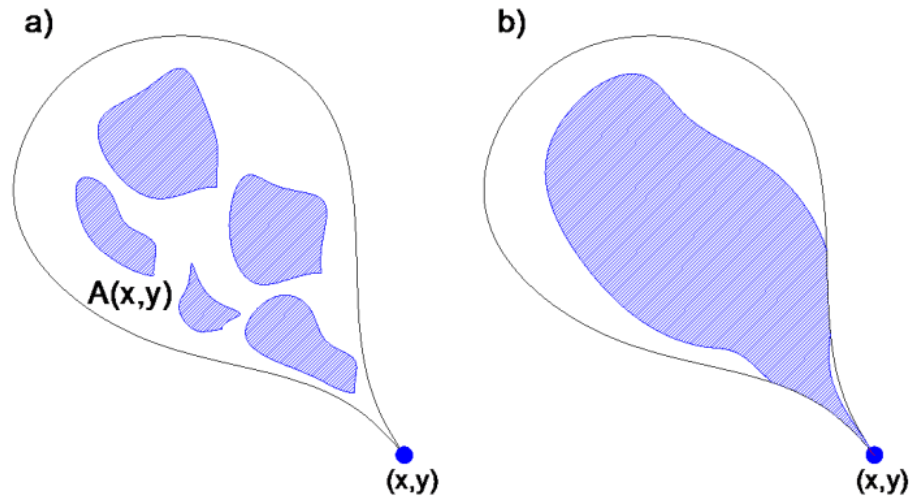
Fig. 2. The concept of hydrological connectivity. Lateral subsurface flow occurs at point (x, y) when this becomes hydrologically connected with its own upslope contributing area $A(x, y)$.

Fig. 3. $\theta_i(z)$ and $\psi_i(z)$ are, respectively, the initial water content and the initial suction head vertical profiles. $\theta_{wt}(z)$ and $\psi_{wt}(z)$ represents the linear water content and suction head vertical profiles associated with zero-suction head at the soil-bedrock interface.
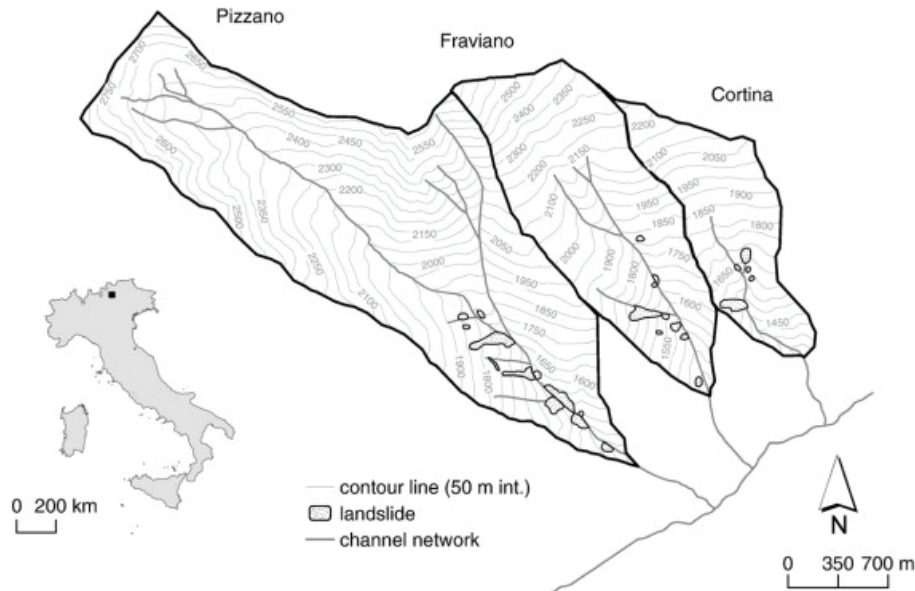
Fig. 4. Catchments case study. The map shows the location of the three catchments, and the landslide distribution (polygons inside the catchments).

Level of Susceptibility

■ very high (Tr<10 years)

■ high (Tr=10-30 years)

■ medium (Tr=30-100 years)

■ low (Tr>100 years)

■ unconditionally stable
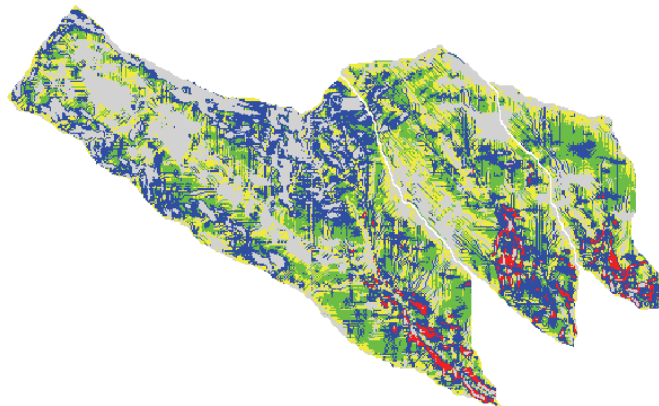
Fig. 5. Patterns of Return period T_R (years) of the critical rainfalls for shallow landslide triggering (i.e., FS ≤ 1) and associated levels of landslide susceptibility.
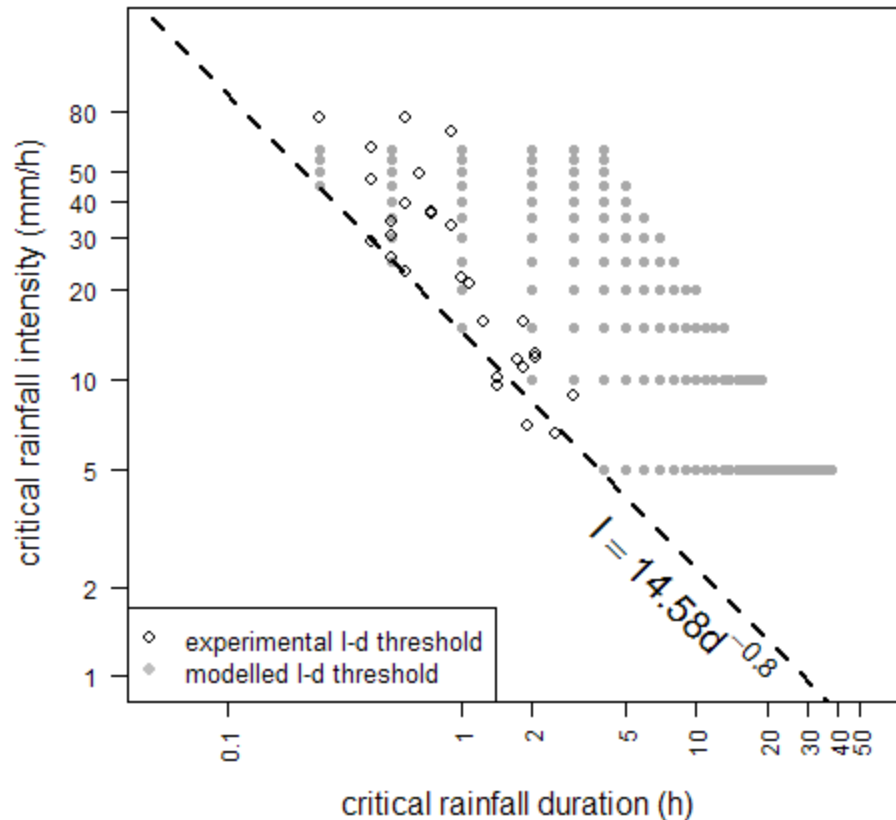
Fig. 6. Modeled local rainfall intensity-duration ($I - d_c$) thresholds for shallow landslide initiation at the three investigated catchments, and experimental $I - d$ that triggered debris flow in some alpine catchments (of the Dolomites) similar to our study area.
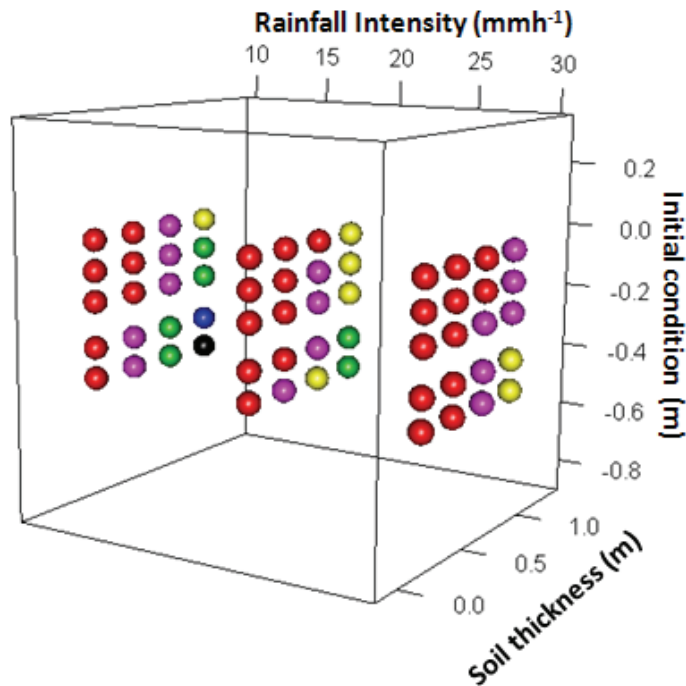
Fig. A1. The balls in the three dimensional space represent the differences between t_{wt} computed with HYDRUS-1D and t_{wt} computed with our simplified infiltration model for 50 scenarios obtained by combining different values of soil thickness, rainfall intensity, and initial pore pressure profile.

Title Page

Abstract | Introduction

Conclusions | References

Tables | Figures

I◄ | ►I

◄ | ►

Back | Close

Full Screen / Esc

Printer-friendly Version

Interactive Discussion